ELSEVIER

1 January 1998

Optics Communications 145 (1998) 159–165

OPTICS COMMUNICATIONS

Resonant patterns in a two-component optical system with 2-D feedback

Boris Y. Rubinstein [1], Len M. Pismen

Department of Chemical Engineering and Minerva Center for Research in Nonlinear Phenomena, Technion - I.I.T., Technion City, Haifa 32 000, Israel

Received 26 June 1997; revised 18 August 1997; accepted 19 August 1997

Abstract

New types of patterns in the transverse profile of an optical beam circulating in a optical system with two nonlinear Kerr slices are reported. Quasicrystalline patterns that may exhibit oscillations on a slow time scale appear as a result of resonant interaction between Turing (stationary) and wave modes. Amplitude equation describing the dynamics of the amplitudes of the excited modes are derived and analyzed. © 1998 Elsevier Science B.V.

PACS: 42.65.Sf
Keywords: Transverse patterns; Resonant interaction; Kerr media; Amplitude equation

1. Introduction

Nonlinear dynamics of coherent light in a media with cubic nonlinearities is extremely diverse. Nonlinear wave interactions produce a variety of dynamical effects like optical multistability [1], chaotic dynamics [2], generation of optical solitons, etc. Spatial effects include spatial amplitude-to-phase conversion, self-focusing and self-defocusing. Another interesting feature is spontaneous pattern formation in the plane transverse to the direction of the light propagation. Optical patterns may be used in the future as data carriers for information processing, provided ways to generate versatile and well controllable patterns are found.

Basic mechanisms of pattern formation are identified through studies of simplified models and corresponding experimental settings. The simplest configuration includes a thin slice of a Kerr-type nonlinear medium coupled to a single feedback mirror. Static (Turing) and dynamic (wave) transverse instabilities in this system have been studied both experimentally [3] and theoretically [4,5]. Static symmetry-breaking instabilities in this simple system always lead to the formation of a stable hexagonal pattern, whereas wave instabilities are strongly damped in slow nonlinear media. The possibility of the wave modes generation was shown in [6] for a single Kerr-slice model.

A variety of transverse patterns, including rolls, hexagons, rotating spirals, and various multipetal structures were observed in experiments with a rotation of the image beam [12–15]. Both periodic and quasicrystalline structures were generated by rotating the image by an angle commensurate with π. Any such structure corresponds to a family of N plane waves with the same wavenumber equispaced in Fourier space. Still more complicated dynamic patterns can be formed by simultaneous excitation of phase-locked Turing and wave modes [15,7]. Selection of quasicrystalline patterns in a feedback cavity has been recently demonstrated analytically and numerically by Leduc et al. [8]. Logvin et al. [9] noticed a possibility of resonance between Turing and wave mode. This resonance has been also detected in Marangoni convection [10].

Another way to enhance the complexity of transverse patterns is to extend the basic single slice system by adding a second Kerr slice and a beam splitter [11].

[1] Corresponding author. E-mail: boris@cekernel.technion.ac.il

PII S0030-4018(97)00471-9

Adding a second slice leads to a complicated structure of neutral curves for both Turing and wave instabilities, facilitating simultaneous excitation of the corresponding plane waves and their resonant interaction.

The aim of this communication is to analyze dynamics of patterns generated through resonant interaction among bifurcating modes of different type. We start (Section 2) with reiterating the linear analysis of the model discussed in Ref. [11], emphasizing simultaneous bifurcation of wave and Turing modes, and continue with the nonlinear analysis and computation of interaction coefficients (Section 3). A resonance condition verified by two wave modes and a single Turing mode leads to complicated spatiotemporal patterns. Coefficients of the amplitude equations describing the pattern dynamics cannot be computed manually due to the complexity of the problem; a special symbolic software [16,17] is used for this purpose.

Following the derivation of amplitude equations, we investigate in Section 4 the long-time dynamics of patterns. A specific feature of the system in question is a possibility to stabilize the pattern by quadratic interactions only. Simple resonant patterns like a hexagonal structure, require for their stability a cubic (four-wave) interaction term to be included, because quadratic (three-wave) terms alone cannot provide an amplitude saturation. We shall see that composite patterns formed by two resonantly interacting modes may be stabilized by three-wave interactions in a wide parametric range, and show that the amplitudes of the constituent modes may undergo slow periodic modulation resulting in complicated spatio-temporal pattern dynamics.

2. Basic equations and linear analysis

The optical system shown in Fig. 1 consists of two Kerr slices S1 and S2, a mirror M, and a beam splitter BS coupling the two nonlinear elements. We assume that the incident beams A_u and A_v are orthogonally polarized, so that their interference can be neglected.

The equations governing the material dynamics [4,11] are derived as a generalization of the model of a single-slice system:

$$\dot{u} + u - \nabla^2 u = K_1 |\mathscr{D}(L_1)\, e^{iu}|^2 + K_2 |\mathscr{D}(L_2)\, e^{iv}|^2,$$
$$\tau \dot{v} + v - \delta^2 \nabla^2 v = \chi K_1 |\mathscr{D}(L_2)\, e^{iu}|^2. \quad (1)$$

Here u and v denote the nonlinear phase modulation introduced by the first and the second slice, respectively; δ^2, τ denote the material diffusivity and the characteristic relaxation time of second slice; the corresponding values for the first slice are normalized to unity by rescaling. The coefficients $K_j\,(j = 1,2)$, are proportional to the intensities of the corresponding incident beams; χ is the ratio of nonlinear sensitivities of the two slices.

The free space propagation of the beams is described by the linear operators $\mathscr{D}(L_j) = \exp(iL_j\nabla^2)$, where L_1 is twice the distance between S1 and the mirror M, and L_2 is the distance between the two slices; ∇^2 denotes the two-dimensional transverse Laplacian. The coordinate in the direction of propagation is scaled by the length L of the diffractional path, and the transverse coordinates, by the diffractional length $\sqrt{L\lambda}$, where λ is the wavelength. When the operator $\mathscr{D}$ acts upon a pure mode with a transverse wave number q, the result is written as $\mathscr{D}(L_j) = \exp(-iq^2 L_j)$. The model (1) is valid under the assumption that the material response time is much larger than the round-trip time in the optical system.

Eq. (1) always has a stationary homogeneous solution $u_0 = K_1 + K_2$, $v_0 = \chi K_1$ which, however, may lose stability when the input intensity exceeds a certain critical level. The critical intensity, as well as the preferred transverse wavelength of the emerging pattern is determined by linear stability analysis of the homogeneous solution.

The standard procedure of linear analysis involves testing stability to arbitrary infinitesimal perturbations, usually plane waves [11]. Proceeding in a standard way, we present the two-component state vector $\boldsymbol{w} = \{u,v\}$ as

$$\boldsymbol{w} = \boldsymbol{w}_0 + \epsilon \boldsymbol{w}_1(\boldsymbol{r},t), \quad (2)$$

where $\epsilon \ll 1$, and linearize Eq. (1) expressing the linear term through Fourier modes $\boldsymbol{w}_1 \sim \exp(i\boldsymbol{q}\boldsymbol{r} + \lambda t)$ with a wave vector $\boldsymbol{q}$. The eigenvalue problem for $\boldsymbol{w}_1$ is written in the form $\mathbf{M}\boldsymbol{w}_1 = 0$ with the matrix

$$\mathbf{M} = \begin{pmatrix} 1 + \lambda + q^2 - 2K_1 \sin L_1 q^2 & -2K_2 \sin L_2 q^2 \\ -2\chi K_1 \sin L_2 q^2 & 1 + \tau\lambda + \delta^2 q^2 \end{pmatrix}. \quad (3)$$

The dispersion relation $\lambda(q)$ is obtained from the equation

$$\det\mathbf{M} = \tau\lambda^2 + \alpha\lambda + \beta = 0, \quad (4)$$

where

$$\alpha = 1 + \delta^2 q^2 + \tau\left(1 + q^2 - 2K_1 \sin q^2 L_1\right),$$
$$\beta = \left(1 + q^2 - 2K_1 \sin q^2 L_1\right)\left(1 + \delta^2 q^2\right) - 4K_1 K_2 \chi \sin q^2 L_2. \quad (5)$$

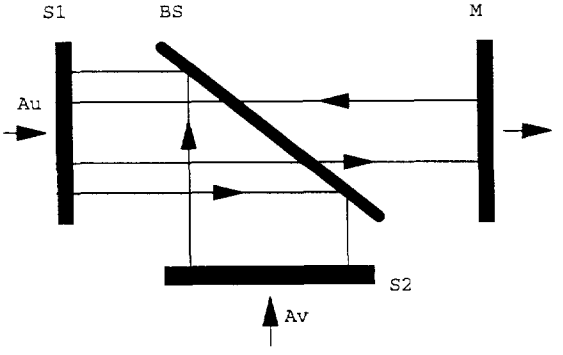

Fig. 1. Scheme of the two-component system.

The condition of Turing instability is $\beta = 0$, $\alpha > 0$, and the condition of wave instability is $\alpha = 0$, $\beta > 0$.

It is convenient to define a *neutral curve* showing the value of one of parameters of the problem, say, K_1, determined by the condition $\mathrm{Re}\ \lambda(q, K_1) = 0$. The neutral curve for the Turing instability is

$$K_1 = \frac{(1+\delta^2 q^2)(1+q^2)}{2(1+\delta^2 q^2)\sin L_1 q^2 + 2\chi K_2 \sin^2 L_2 q^2}, \tag{6}$$

The lowest minimum of this curve K_s determines the critical wavenumber $q_s = Q$. We denote the eigenvector of the matrix $\mathbf{M}$ at $K_1 = K_s$, $\lambda = 0$, $q = Q$ as $\boldsymbol{U}_s$. Due to the rotational degeneracy in an isotropic system, excitation of several plane waves with the same wavenumber Q but different directions is possible. Thus the linear planform may be written as follows:

$$\boldsymbol{w}_1 = \boldsymbol{U}_s \sum_{j=1}^{N} a_j e^{i\boldsymbol{Q}_j \boldsymbol{r}} + \text{c.c.}, \tag{7}$$

where a_j is a complex amplitude of the plane wave with the wave vector $\boldsymbol{Q}_j$, and $|\boldsymbol{Q}_j| = Q$.

The wave instability is characterized by the following neutral stability curve:

$$K_1 = \frac{1+\tau+q^2(\tau+\delta^2)}{2\sin L_1 q^2}, \tag{8}$$

with the critical wavenumber $q_w = k$ corresponding to the absolute minimum K_w of Eq. (8). The frequency is computed as

$$\omega^2 = (1+\delta^2 k^2)(1+k^2 - 2K_w \sin L_1 k^2) - 4\chi K_w K_2 \sin^2 L_2 k^2. \tag{9}$$

The eigenvector of $\mathbf{M}$ at this point is denoted as $\boldsymbol{U}_w$. The general planform is

$$\boldsymbol{w}_1 = \boldsymbol{U}_w \sum_{j=1}^{N} b_j e^{i(\boldsymbol{k}_j \boldsymbol{r} + \omega t)} + \text{c.c.}, \tag{10}$$

The minima of the neutral curves (6, 8) are determined by transcendental equations, and cannot be found analytically, but one can locate numerically a degenerate point where $K_s = K_w$, and both Turing and wave modes are excited simultaneously. Fig. 2 demonstrates an interchange of the minima of the neutral curves due to a slight shift of the distance L_1.

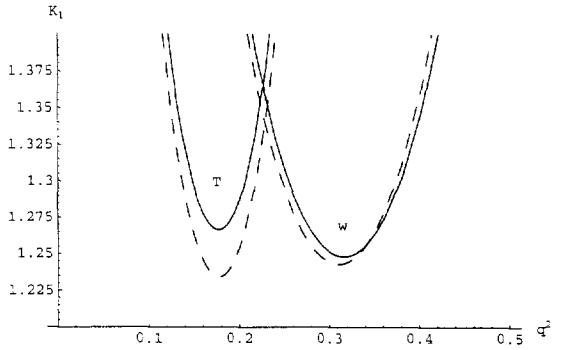

Fig. 2. The first branches of the neutral curve for Turing (T) and wave (w) instabilities calculated at $L_1 = 4.55$ (solid line) and $L_1 = 4.65$ (dashed line). The absolute minima are interchanged through a small shift of the parameter. The values of other parameters are: $\tau = 1$, $L_2 = 1$, $K_2 = 1$, $\delta^2 = 0.5$, $\chi = -4.5$.

3. Weakly nonlinear analysis

3.1. Multiscale expansion

The nonlinear analysis is carried out following the standard method of multiscale expansion [17]. We introduce a hierarchy of time scales:

$$\partial/\partial t = \partial/\partial t_0 + \epsilon \partial/\partial t_1 + \epsilon^2 \partial/\partial t_2 + \ldots, \tag{11}$$

and expand in Taylor series the state variable and the bifurcation parameter:

$$\boldsymbol{w} = \boldsymbol{w}_0 + \epsilon \boldsymbol{w}_1 + \epsilon^2 \boldsymbol{w}_2 + \ldots,$$
$$K_1 = K_{10} + \epsilon K_{11} + \epsilon^2 K_{12} + \ldots. \tag{12}$$

In order to exclude the dependence of the basic solution $\boldsymbol{w}_0$ on the bifurcation parameter, we shift the variable $\boldsymbol{w} \to \boldsymbol{w} - \boldsymbol{w}_0$; then Eq. (1) becomes

$$\mathbf{T}\dot{\boldsymbol{w}} - \mathbf{D}\nabla^2 \boldsymbol{w} + \boldsymbol{w} + \boldsymbol{w}_0 = \mathbf{N}_1 |e^{iL_1\nabla^2} e^{i\boldsymbol{w}}|^2 + \mathbf{N}_2 |e^{iL_2\nabla^2} e^{i\boldsymbol{w}}|^2, \tag{13}$$

with the trivial basic solution $\boldsymbol{w} = 0$. Here $\mathbf{T} = \mathrm{diag}(1, \tau)$, $\mathbf{D} = \mathrm{diag}(1, \delta^2)$, and $\mathbf{N}_j$ are the third rank tensors of the form:

$$\mathbf{N}_1 = \begin{pmatrix} (K_1, 0) & (0,0) \\ (0,0) & (0,0) \end{pmatrix},$$
$$\mathbf{N}_2 = \begin{pmatrix} (0,0) & (0, K_2) \\ (\chi K_1, 0) & (0,0) \end{pmatrix}. \tag{14}$$

Using the above expansions in Eq. (13) we recover in the first order in ϵ the linear eigenvalue problem in the following form

$$\mathscr{L}\boldsymbol{w}_1 \equiv \left[\mathbf{T}\partial/\partial t_0 + \mathbf{I} - \mathbf{D}\nabla^2 + 2\left(\mathbf{N}_{10}\sin L_1 \nabla^2 + \mathbf{N}_{20}\sin L_2 \nabla^2\right)\mathbf{I}_1\right]\boldsymbol{w}_1 = 0, \tag{15}$$

where $\mathbf{I}$ is the identity matrix, and $\mathbf{I}_1$ is the vector $\{1,1\}$. The tensors $\mathbf{N}_{j0}$ are calculated at $K_1 = K_{10}$. The linear operator $\mathscr{L}$ must be determined for both Turing ($\mathscr{L}_s$) and wave ($\mathscr{L}_w$) instability as follows:

$$\mathscr{L}_s = \mathscr{L}(K_{10} = K_s, \nabla \to iQ, \partial/\partial t_0 \to 0),$$
$$\mathscr{L}_w = \mathscr{L}(K_{10} = K_w, \nabla \to ik, \partial/\partial t_0 \to i\omega). \tag{16}$$

In the next order in ϵ, we arrive at the following inhomogeneous linear problem:

$$\mathscr{L}\boldsymbol{w}_2 = -\mathbf{T}\partial\boldsymbol{w}_1/\partial t_1 + 2\left(\mathbf{N}_{10}\sin^2\left(L_1\nabla^2/2\right) + \mathbf{N}_{20}\sin^2\left(L_2\nabla^2/2\right)\right)\boldsymbol{w}_1^2 - 2\left(\mathbf{N}_{11}\sin\left(L_1\nabla^2\right) + \mathbf{N}_{21}\sin\left(L_2\nabla^2\right)\right)\mathbf{I}_1\boldsymbol{w}_1. \quad (17)$$

Here the tensors $\mathbf{N}_{j1}$ are obtained from $\mathbf{N}_j$ by replacing $K_1 \to K_{11}$.

The amplitude equations are obtained as solvability conditions of Eq. (17), i.e., conditions of orthogonality of the inhomogeneity to all eigenfunctions of the adjoint linear problem. A nontrivial solvability condition is obtained when the quadratic term (a product of two eigenfunctions, say, ψ_1 and ψ_2) is *in resonance* with a another eigenmode, say, ψ_0. This requires that the frequencies and wavenumbers of the three modes involved satisfy the conditions

$$\boldsymbol{k}_1 + \boldsymbol{k}_2 = \boldsymbol{k}_0, \quad \omega_1 + \omega_2 = \omega_0. \quad (18)$$

A resonance triplet may involve therefore either three Turing modes or two wave modes from the same family (i.e., with identical frequencies) and one Turing mode.

3.2. Basic resonant structure

A possible resonant structure consists of two wave modes with a wavenumber k and one Turing mode with the wavenumber Q. The pattern in the Fourier space is an isosceles triangle (and its conjugate produced by rotating the original triangle by π). Altogether, this resonant planform is built of three plane wave modes:

$$\boldsymbol{w}_1 = a\,\mathrm{e}^{i\boldsymbol{Q}\boldsymbol{r}}\boldsymbol{U}_s + \mathrm{e}^{i\omega t}\left(b\,\mathrm{e}^{i\boldsymbol{k}_1\boldsymbol{r}} + c\,\mathrm{e}^{i\boldsymbol{k}_2\boldsymbol{r}}\right)\boldsymbol{U}_w + \mathrm{c.c.}, \quad (19)$$

where the resonance condition (18) is satisfied: $\boldsymbol{k}_1 - \boldsymbol{k}_2 = \boldsymbol{Q}$. A snapshot of this pattern reconstructed using the amplitude equations solutions discussed below is shown in Fig. 3.

In order to derive dynamic equations for the amplitudes a,b and c, one has to substitute (19) in the r.h.s. of Eq. (17), and then to project it on the adjoint eigenvectors $\boldsymbol{U}_s^\dagger, \boldsymbol{U}_w^\dagger$ satisfying $\mathscr{L}_s^\dagger\boldsymbol{U}_s^\dagger = 0$, $\mathscr{L}_w^\dagger\boldsymbol{U}_w^\dagger = 0$, where $\mathscr{L}_{s,w}^\dagger = \mathscr{L}_{s,w}^*$ are the operators adjoint to $\mathscr{L}_{s,w}$.

After some algebra, we arrive at the following system of amplitude equations:

$$\dot{a} = \mu_s a + \nu_s bc^*, \quad \dot{b} = \mu_w b + \nu_w ac, \quad \dot{c} = \mu_w c + \nu_w a^* b, \quad (20)$$

where μ_s and ν_s are real, while μ_w and ν_w are complex. These coefficients are defined as

$$\mu_s = 2\boldsymbol{U}_s\mathbf{I}_1\left(\mathbf{N}_{11}\sin L_1Q^2 + \mathbf{N}_{21}\sin L_2Q^2\right)\boldsymbol{U}_s^\dagger/\left(\boldsymbol{U}_s\mathbf{T}\boldsymbol{U}_s^\dagger\right),$$
$$\mu_w = 2\boldsymbol{U}_w\mathbf{I}_1\left(\mathbf{N}_{11}\sin L_1k^2 + \mathbf{N}_{21}\sin L_2k^2\right)\boldsymbol{U}_w^\dagger/\left(\boldsymbol{U}_w\mathbf{T}\boldsymbol{U}_w^\dagger\right),$$
$$\nu_s = 2\boldsymbol{U}_w\boldsymbol{U}_w^*\left(\mathbf{N}_{10}\sin^2L_1Q^2/2 + \mathbf{N}_{20}\sin^2L_2Q^2/2\right)\boldsymbol{U}_s^\dagger/\left(\boldsymbol{U}_s\mathbf{T}\boldsymbol{U}_s^\dagger\right),$$
$$\nu_w = 2\boldsymbol{U}_s\boldsymbol{U}_w\left(\mathbf{N}_{10}\sin^2L_1k^2/2 + \mathbf{N}_{20}\sin^2L_2k^2/2\right)\boldsymbol{U}_w^\dagger/\left(\boldsymbol{U}_w\mathbf{T}\boldsymbol{U}_w^\dagger\right). \quad (21)$$

They are computed numerically with the help of our bifurcation package [16,17].

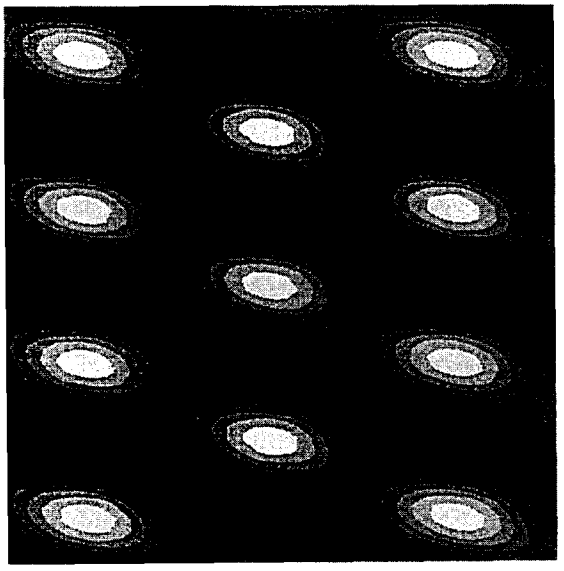

Fig. 3. A snapshot of the reconstructed pattern corresponding to the planform (19) calculated at $\tau = 1$, $L_1 = 1.5$, $L_2 = 1$, $K_1 = 3.169$, $K_2 = 0.159$, $\delta = 2$, $\chi = -18.55$.

3.3. Closed resonant structure

It appears that the above structure is unstable to excitation of additional resonant modes, and, hence, it can be viewed only as a basic building block of more complex structures in the Fourier space. A single isosceles triangle can be complemented by one Turing and one wave modes in such a way to a new structure comprised of two isosceles triangles with one common side. Still more complicated structures can be constructed in a similar way.

The acute angle between two wave modes in the basic triangle, which is determined by the ratio of the wavenumbers of the Turing and wave modes can be changed smoothly within a certain range by tuning the free parameters of the model. When the angle becomes commensurate with π, one can also envisage a closed rotationally invariant structure comprised of $2N$ isosceles triangles. The corresponding planform is given by:

$$\boldsymbol{w}_1 = \sum_{j=1}^{N}\left(a_{1,j}\,\mathrm{e}^{i\boldsymbol{Q}_{1,j}\boldsymbol{r}} + a_{2,j}\,\mathrm{e}^{i\boldsymbol{Q}_{2,j}\boldsymbol{r}}\right)\boldsymbol{U}_s + \mathrm{e}^{i\omega t}\left(b_j\,\mathrm{e}^{i\boldsymbol{k}_{1,j}\boldsymbol{r}} + c_j\,\mathrm{e}^{i\boldsymbol{k}_{2,j}\boldsymbol{r}}\right)\boldsymbol{U}_w + \mathrm{c.c.}, \quad (22)$$

where the following conditions are satisfied:

$$\boldsymbol{k}_{1,j} - \boldsymbol{k}_{2,j} = \boldsymbol{Q}_{1,j}, \quad \boldsymbol{k}_{1,j+1} - \boldsymbol{k}_{2,j} = \boldsymbol{Q}_{2,j}.$$

Assuming that $a_{1,j} = a_{2,j} = a$, $b_j = b$, and $c_j = c$ we arrive at the dynamical system similar to (20) with the only replacement $\nu_w \to 2\nu_w$. This means that both cases can be analyzed simultaneously.

A snapshot of a rotationally invariant pattern with $N = 4$ and the corresponding structure in the Fourier space are shown in Fig. 4.

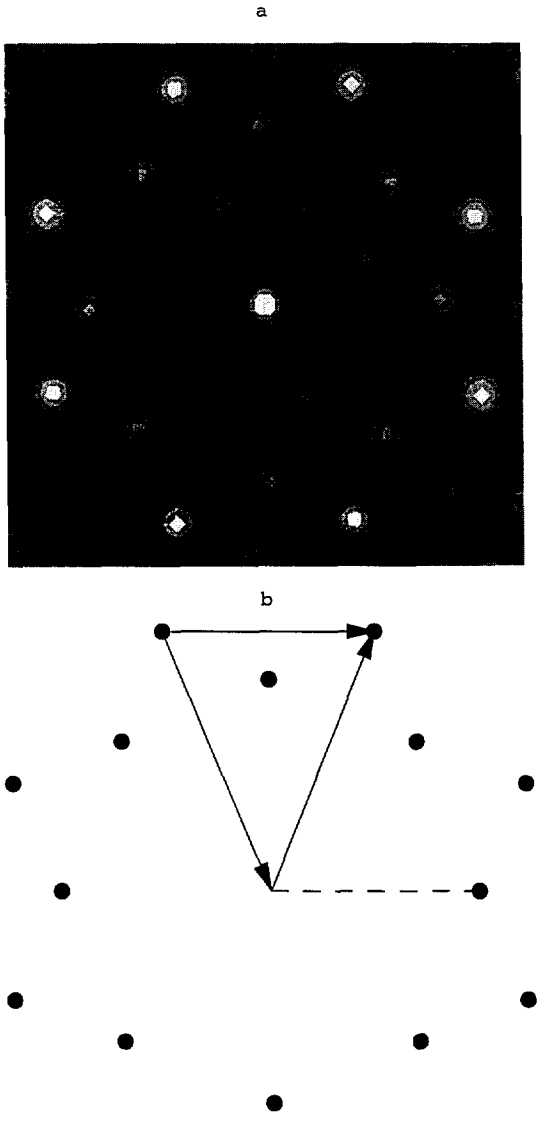

Fig. 4. The planform (22) calculated at $\tau = 1$, $L_1 = 1.5$, $L_2 = 1$, $K_1 = 3.169$, $K_2 = 0.159$, $\delta = 2$, $\chi = -18.55$. (a) A snapshot of the real space (near field) image. (b) The structure in the Fourier space (far field image). The inner circle corresponds to Turing modes, and the outer circle, to wave modes. One of the resonance isosceles triangles is shown, and the participating Turing mode is indicated by the dashed line.

If the required value of the angle is reached only approximately, we can consider the same closed structure but take into account that the excited modes may have wavenumbers slightly different from the exact minima of the neutral curves. We call such structure a *strained* closed resonance. It means that if the acute angle between two wave modes in the basic triangle is incommensurate with π, its value can be approximated by some rational fraction of π, and one may expect excitation of strained closed resonant structure.

4. Amplitude dynamics

The amplitude equations involving three modes have interesting dynamics. It is advantageous to use the polar representation of the complex amplitudes,

$$a = \rho_a e^{i\theta_a}, \quad b = \rho_b e^{i\theta_b}, \quad c = \rho_c e^{i\theta_c}. \tag{23}$$

Then Eqs. (20) is reduced to the following system of four real equations including a single phase combination $\theta = \theta_a + \theta_c - \theta_b$:

$$\begin{aligned}
\dot{\rho}_a &= \mu_s \rho_a + \nu_s \rho_b \rho_c \cos\theta, \\
\dot{\rho}_b &= \mu_w \rho_b + \nu \rho_a \rho_c \cos(\theta - \alpha), \\
\dot{\rho}_c &= \mu_w \rho_c + \nu \rho_a \rho_b \cos(\theta + \alpha), \\
\dot{\theta} &= -\nu_s \frac{\rho_b \rho_c}{\rho_a} \sin\theta - \nu \frac{\rho_a \rho_b}{\rho_c} \sin(\theta + \alpha) \\
&\quad - \nu \frac{\rho_a \rho_c}{\rho_b} \sin(\theta - \alpha),
\end{aligned} \tag{24}$$

where $\nu_w = \nu e^{-i\alpha}$, and μ_w denotes the real part of the coefficient given by (21).

The stationary values of the amplitudes ρ_a, ρ_b, ρ_c can be expressed as

$$\begin{aligned}
\rho_a &= \frac{\mu_w}{\nu\sqrt{\cos(\theta - \alpha)\cos(\theta + \alpha)}}, \\
\rho_{b,c} &= \sqrt{\frac{\mu_s \mu_w}{\nu\nu_s \cos(\theta \pm \alpha)\cos\theta}}.
\end{aligned} \tag{25}$$

The stationary value of the phase θ verifies the following equation:

$$\tan\theta + \frac{\mu \sin 2\theta}{\cos(\theta - \alpha)\cos(\theta + \alpha)} = 0, \tag{26}$$

where $\mu = \mu_w/\mu_s$. A simple solution of this equation satisfies $\sin\theta = 0$, yielding $\theta = \pi$ at $\mu_s \nu_s > 0$ and $\mu_w \cos\alpha > 0$, and $\theta = 0$ for the opposite sign of these products. This is a symmetric solution with equal amplitudes of the wave modes: $\rho_b = \rho_c = \sqrt{\mu_s \mu_w / (\nu\nu_s \cos\alpha)}$. Applying the Routh–Hurwitz stability criterion one can check that the stability conditions of the symmetric solution are

$$\mu_w > 0, \quad \mu > -\tfrac{1}{4}, \quad \mu_s < -\tfrac{1}{2}\cos^2\alpha. \tag{27}$$

Another solution of Eq. (26) verifies the relation

$$\cos^2\theta = \frac{\sin^2\alpha}{1+2\mu}. \tag{28}$$

It is immediately seen that the solution exists provided $\mu > -\frac{1}{2}$ and $1+2\mu \geq \sin^2\alpha$, which leads to the condition $\mu \geq -\frac{1}{2}\cos^2\alpha$. It is required for positiveness of the amplitudes that $\cos(\theta-\alpha)\cos(\theta+\alpha) > 0$. This inequality can be rewritten in the form $\mu\sin^2\alpha < 0$, and hence, $\mu < 0$. Eq. (28) defines in fact a pair of asymmetric solutions which are transformed one to the other by interchanging the amplitudes of the wave modes. This pair bifurcates from the symmetric solution at $\mu = -\frac{1}{2}\cos^2\alpha$. The bifurcation is supercritical at $\mu > -\frac{1}{4}$.

At still higher values of μ, the asymmetric solutions undergoes a supercritical Hopf bifurcation. The bifurcation locus in the plane (α,μ) is given implicitly by the relation

$$-(1+4\mu)(1+5\mu+8\mu^2)\sin^4\alpha + 3(4+7\mu+4\mu^2) \times (2\mu+\cos^2\alpha)^2 + [3+8\mu(\mu+2)(1+2\mu)] (2\mu+\cos^2\alpha)\sin^2\alpha = 0. \tag{29}$$

The additional stability condition is $\mu_s < 0$.

A bounded periodic solution (see Fig. 5) that exists beyond this curve further disappears as a result of a saddle-loop bifurcation. We were unable to determine the locus of this bifurcation exactly because of a very complicated dynamics in the vicinity of a saddle point in the four-dimensional phase space. This is a saddle-focus with two-dimensional stable and unstable manifolds, both oscillatory. Our numerical estimates suggest that the saddle-loop boundary is roughly defined by the relation $\mu = -\pi\alpha$. On the other side of this boundary, the dynamics is apt to be chaotic. A period doubling of the symmetric periodic solution is observed close to the double zero singularity at

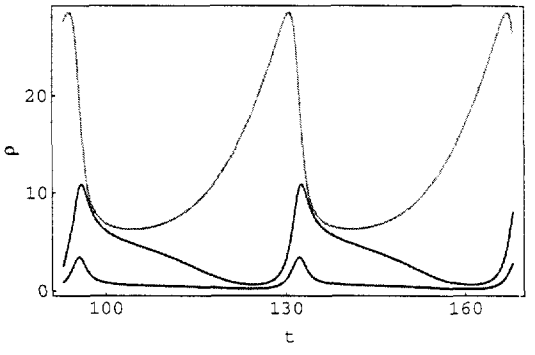

Fig. 5. A periodic solution of the system Eq. (24) for at $\mu_w/\mu_s = -0.0238$, $\nu_s = 0.0678$, $\nu = 0.3523$, $\alpha = -0.66\pi$. Two periods of oscillations are shown. The amplitude of the Turing mode ρ_a is much smaller than the wave mode amplitudes ρ_b and ρ_c.

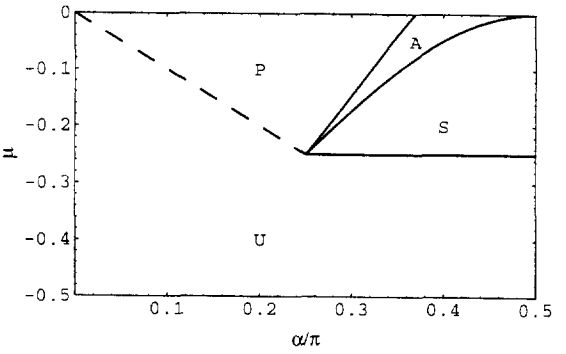

Fig. 6. Bifurcation diagram of Eq. (24) in the parametric plane (α,μ) for $\mu_s < 0$, $\nu_s < 0$. Letters S and A denote the regions of stable stationary symmetric and asymmetric solutions; P stands for a pair of periodic solutions, and U for a symmetric periodic solution or other symmetric dynamic attractor. The dashed line shows an approximate location of the saddle-loop bifurcation.

$\mu = 1/4$, $\alpha = \pi/4$. At $\mu > 0$, i.e. $\mu_s < 0$ and $\mu_w < 0$ the pattern decays to the trivial featureless state. With $\mu_s > 0$ and $\mu_w > 0$ the amplitudes grow infinitely which invalids the Eq. (20). The resulting bifurcation diagram in the plane (α,μ) is presented in Fig. 6. The picture in the range $\pi/2 < \alpha \leq \pi$ is symmetric relative to the axis $\alpha = \pi/2$.

While an asymmetric periodic solution cannot transcend the saddle point, there are no apriori limits on the amplitude of symmetric oscillations, which tends to grow as μ becomes more negative. Confinement in small-amplitude region by quadratic interactions is only possible when the Turing mode is subcritical and the wave mode is supercritical but not too strongly. When runaway to large amplitudes is observed, the actual pattern may be stabilized by non-resonant cubic interactions. The planform determined by (19) has a complicated non-stationary quasicrystalline structure. The amplitudes may be subject to slow periodic modulation when the dynamics is periodic. Fig. 5 shows an example of the periodic solution of Eq. (24). During each period of oscillations there is a short time interval when $\rho_b \approx \rho_c$, and the corresponding pattern (22) is quasicrystalline and looks similar to that of shown in Fig. 4(a). Then one wave mode amplitude becomes larger and the other tends to smaller values what leads to distortion of the pattern. Finally, the smaller amplitude reaches its minimum, and the transformation into a square pattern takes place.

5. Conclusion

In this paper we reported new types of the resonant patterns arising in a two-component system with two-dimensional feedback. The model provides a possibility of the simultaneous excitation of bifurcating modes of differ-

ent types. A resonant interaction of these modes produces complex transversal patterns with nontrivial dynamics.

A basic resonance structure of new type can be presented in the Fourier space as an isosceles triangle with a Turing mode playing role of its base, and the lateral sides are the wave modes. This structure can be viewed as a basic building block of more complex structures in the Fourier space. If the acute angle between the wave modes is commensurate with π, the closed rotationally invariant structure comprised of even number of basic triangles can be envisaged.

We showed that the dynamics of the modes in the basic (single triangle) structure and the closed structure are the same. It gives us a comparatively simple way of the analysis of the pattern dynamics. Three main types of the dynamics were detected. There exist a stationary symmetric solution with the wave mode amplitudes equal one to another, it corresponds to the quasicrystalline pattern for closed Fourier space structure. Another type of the stationary solution is characterized by the unequal wave amplitudes and the distorted pattern. There is also a solution corresponding to the periodic oscillation of the mode amplitudes what leads to a slow modulation of the pattern. It evolves into a cycle between the quasicrystalline and the square structures.

Simple resonant patterns like hexagons require a cubic terms for their stability. A novel feature of the considered resonant patterns is a possibility of their stabilization by the quadratic interactions only.

References

[1] H.M. Gibbs, Optical Bistability: Controlling Light with Light (Academic, New York, 1985).
[2] K. Ikeda, A. Daido, O. Akimoto, Phys. Rev. Lett. 45 (1982) 709.
[3] R. Macdonald, H.J. Eichler, Optics Comm. 89 (1992) 289.
[4] J. D'Alessandro, W.J. Firth, Phys. Rev. A 46 (1992) 537.
[5] M.A. Vorontsov, W.J. Firth, Phys. Rev. A 49 (1992) 2891.
[6] W.J. Firth, J. Mod. Optics 37 (1990) 151.
[7] B.Y. Rubinstein, L.M. Pismen, submitted to Phys. Rev. A (1997).
[8] D. Leduc, M. Le Berre, E. Ressayre, A. Tallet, Phys. Rev. A 53 (1996) 1072.
[9] Yu. A. Logvin, B.A. Samson, A.A. Afanas'ev, A.M. Samson, N.A. Loiko, Phys. Rev. E 54 (1996) R4548.
[10] P. Colinet, Ph. Géoris, J.C. Legros, G. Lebont, Phys. Rev. E 54 (1996) 514.
[11] E.V. Degtiarev, V. Watagin, Optics Comm. 124 (1996) 309.
[12] S.A. Akhmanov, M.A. Vorontsov, V.Yu. Ivanov, A.V. Larichev, N.I. Zelenykh, J. Opt. Soc. Am. B 9 (1992) 78.
[13] E. Pampaloni, S. Residori, F.T. Arecchi, Europhys. Lett. 24 (1993) 647.
[14] E. Pampaloni, P.L. Ramazza, S. Residori, F.T. Arecchi, Phys. Rev. Lett. 74 (1995) 258.
[15] E. Pampaloni, S. Residori, S. Soria, F.T. Arecchi, Phys. Rev. Lett. 78 (1997) 1042.
[16] L.M. Pismen, B.Y. Rubinstein, M.G. Velarde, Int. J. of Bifurcations and Chaos 6 (1996) 2163.
[17] L.M. Pismen, B.Y. Rubinstein, Tools for Nonlinear Analysis, preprint chao-dyn/9601017, available at http://xxx.lanl.gov.